Design of a novel fluidized bed reactor to enhance sorbent performance in CO_2 capture systems using CaO

M. Elena Diego[a,], Borja Arias[a], Gemma Grasa[b] and J. Carlos Abanades[a]*

[a]Instituto Nacional del Carbón (CSIC), Francisco Pintado Fe 26, 33011 Oviedo, Spain

[b]Instituto de Carboquímica (CSIC), Miguel Luesma Castán 4, 50018 Zaragoza, Spain

KEYWORDS

CO_2 capture; Calcium Looping; Reactivation; Recarbonation; Bubbling bed reactor

ABSTRACT

This work deals with the modeling and design of a novel bubbling fluidized bed reactor that aims to improve the CO_2 carrying capacity of CaO particles in CO_2 capture systems by Calcium Looping (CaL). Inside the new reactor (the recarbonator) the particles that arrive from the carbonator of the CaL system react with a concentrated stream of CO_2, thereby increasing their carbonate content up to a certain value which can be predicted by means of the model proposed. The recarbonator model presented in this work is based on the Kunii and Levenspiel model for bubbling bed reactors of fine particles. The reduction in the gas volume due to the reaction of

CO_2 with CaO is taken into account by dividing the recarbonator into a number of reactor elements where the bubble properties are recalculated, while the solids are perfectly mixed throughout the bed. The model has been used to test the conceptual design of a CaL system that incorporates an additional recarbonator reactor to more than double the residual CO_2 carrying capacity of the sorbent (from 0.07 to 0.16). In a reference design case of a 1000 MW_{th} coal-fired power plant it was found that the recarbonator cross-section needs to be between 80 and 100 m^2 (about 40-50% the area of the carbonator reactor), the solid inventories around 1200-1500 kg/m^2 and the inlet CO_2 gas velocities between 0.6 and 0.9 m/s. This set of operating and design windows predicts an increase in the carbonate content of the particles in the recarbonator of around 0.02, which has been shown to be sufficient to sustain the increased average CO_2 carrying capacity of the sorbent.

1. INTRODUCTION

CO_2 Capture and Storage (CCS) is one of the major options for contributing to the mitigation of climate change[1], and several processes have been proposed in the last few years aimed at a less costly and more energy efficient capture of CO_2. To this end, postcombustion Calcium Looping (CaL) stands out as a promising technology for CO_2 capture and is attracting increasing interest (see for example recent reviews[2, 3]).

The basis of the CaL process relies on the use of lime as a CO_2 sorbent, which undergoes consecutive carbonation/calcination cycles in the process. The pioneers of this process for combustion systems were Shimizu et al.[4], who proposed a system of two fluidized beds (carbonator and calciner) and a method to regenerate the $CaCO_3$ in the calciner based on burning

a fuel with pure O_2. The main process route today comprises two interconnected circulating fluidized bed (CFB) reactors, namely the carbonator and the calciner (see Figure 1). The carbonator operates at temperatures of around 650ºC and contains active CaO particles which react with the CO_2 of the flue gas entering this reactor. As a result, a CO_2 depleted gas leaves the carbonator and a partially carbonated stream of solids is transported to the calciner for regeneration. The calciner requires temperatures in the range of 880-950ºC to calcine not only the $CaCO_3$ from the carbonator, but also the fresh limestone fed to the system to compensate for the decay of the CO_2 capture capacity of the lime with the number of carbonation/calcination cycles[5, 6]. As mentioned above, the calcination reaction is endothermic and heat is provided by burning coal in oxyfuel conditions inside the reactor. The calcined CaO solid stream is then transported back to the carbonator to initiate a new CO_2 capture cycle.

Provided that an adequate integration of all the heat sources is carried out, the CaL process is competitive and has a low overall energy penalty[4, 7-15]. It has been possible to demonstrate the practical viability of the process at increasing scale in only a few years due to the close similarity of the reactors to those used in well-established circulating fluidized bed combustion technology. Several lab-scale experimental facilities contributed to validate the CaL concept[16-20] and this has led to a rapid development of the process. Postcombustion CaL technology has reached the 1.7 MW_{th} scale with a pilot plant in continuous operation in La Pereda (Spain)[21]. Other pilots have also reported successful results in Germany (in Sttutgart (200 kW_{th})[22] and Darmstadt (1 MW_{th})[23]) or are being commissioned (a 1.9 MW_{th} pilot in Taiwan[24]).

A critical aspect of the CaL system is, as mentioned above, the progressive deactivation experienced by the lime when it is subjected to consecutive cycles of carbonation and calcination[5, 6]. Maintaining high CO_2 capture efficiencies while operating with low CO_2 sorbent carrying capacities requires an increase in the solid circulation rates between the reactors. This imposes high energy penalties on the process due to the rise in the heat requirements of the calciner[25, 26]. Therefore, in the CaL process a continuous make-up flow of fresh limestone has to be fed in to stabilize the activity of the CaO particles at a sufficiently high value. Meanwhile, a continuous purge of solids leaves the system. The presence of a continuous make-up flow also imposes an energy penalty on the process, but this can be reduced if a synergy arrangement can be established with a cement manufacturer. Nonetheless, it is clear that it would be highly beneficial if the amount of fresh limestone required in the CaL process could be reduced. For this purpose, a number of modified sorbents and reactivation techniques are being studied[3, 27].

One of the first strategies proposed to increase the CO_2 carrying capacity of lime was the hydration of CaO particles[28-31], which has been proven to be beneficial for the CO_2 capture capacity of the sorbent. Its main drawbacks are an increase in the tendency towards attrition due to the reduced mechanical stability of the hydrated lime and the energy penalty associated with the generation of large amounts of steam and low temperatures used in the hydration process (compared to those of the CaL system)[32]. Sorbent doping is also a technique which is being studied as an alternative to increase the CO_2 carrying capacity of the CaO particles, but the results obtained so far are not conclusive[27]. The use of synthetic sorbents has also been proposed and recently reviewed by Kierzkowska et al.[27]. The main concerns regarding these Ca-based sorbents are the limited availability of experimental results under operating conditions suitable

for the CaL scheme and the economic impact that these sorbents may have on the process[3, 27, 33]. Finally, several authors have reported self-reactivation effects[34-39] during laboratory tests at large carbonation time scales or intense carbonation conditions. However, these effects are not expected to occur in postcombustion CaL applications because the intrinsic operating conditions do not allow such long solids residence times in the reactor or such carbonation conditions[40].

This work focuses on a novel recarbonation process[41, 42] that is also aimed at improving the CO_2 carrying capacity of the sorbent like the methods referred to in the previous paragraph. In this case, the reactivation concept is based on experimental evidence that extended carbonation times result in higher residual activities of lime[34, 43, 44]. In 1973, multicycle carbonation/calcination tests carried out by Barker[43] for carbonation times of 24 hours in pure CO_2 revealed no significant decay in CO_2 carrying capacity (approx. 0.82 after 10 cycles). Further trials by Gottipati to reactivate spent sorbent for SO_2 capture using CO_2 failed to achieve the desired gains[45]. Nevertheless, more recent experiments focused on Ca looping systems under more moderate conditions than those of Barker[43](which are not suitable for large-scale continuous systems due to the long reaction times and carbonation conditions), have confirmed that prolonged carbonation times increase the residual activity of the CaO compared to experiments performed for short carbonation times[34, 43, 44]. High CO_2 partial pressures have also been shown to be beneficial for enhancing the reactivation of lime[46].

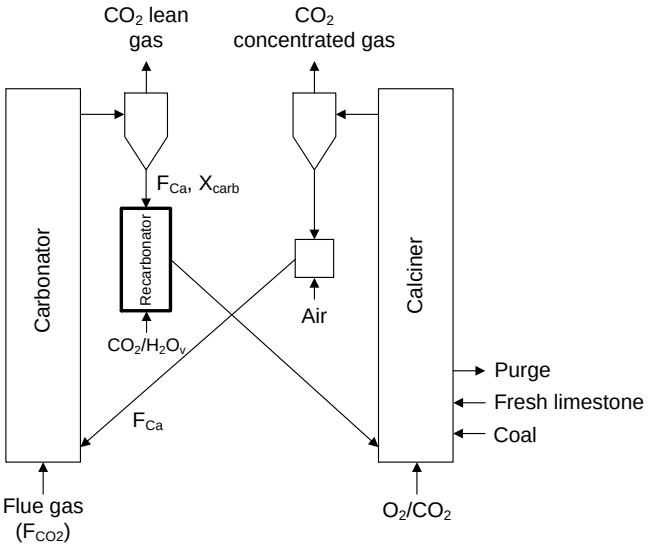

Figure 1. General scheme of a postcombustion calcium looping system that incorporates a bubbling fluidized bed recarbonator reactor to increase the CO_2 carrying capacity of the sorbent (CaO).

In previous works[41, 42] we proposed a variation of the CaL CO_2 capture system that incorporates a new recarbonator reactor located between the carbonator and the calciner (see Figure 1). The recarbonator reactor, which is expected to operate at temperatures of between 750-850ºC, is fed with partially carbonated solids from the carbonator and a highly CO_2 concentrated gas stream. As a result, the particles are forced to increase their carbonate content beyond their maximum carrying capacity in the carbonator ($X_{ave,R}$) to a new higher value. In a stationary state, the resulting increase in the carbonate content in the recarbonator (ΔX_R) with respect to $X_{ave,R}$ is enough to compensate for the subsequent decrease in the CO_2 carrying capacity the particles experience in the next calcination cycle. In these conditions, $X_{ave,R}$ retains the same value as at the exit of the carbonator. However, it is feasible in these conditions to stabilize the average maximum carrying capacity of the particles ($X_{ave,R}$) at values considerably higher than those reached in a classic CaL scheme without recarbonation (X_{ave}). In fact, it has

been estimated from experimental measurements using thermogravimetric equipment that a ΔX_R as low as 0.02 may provide a residual activity of lime (X_r) equal to 0.16[41, 47] whereas the original X_r without recarbonation is only between 0.07 and 0.10.

The purpose of this paper is to establish a first reactor design for the recarbonator reactor taking into account the typical operating conditions that can be expected in large-scale CaL systems, the information available on recarbonation kinetics and bubbling bed reactor gas-solid contact quality. Short solids residence times are likely to be needed in the recarbonator reactor to keep to reasonable dimensions, since a large solid circulation rate between the carbonator and the calciner reactors can always be expected if a high CO_2 capture efficiency is to be maintained. Therefore, a reactor model incorporating recent knowledge on the kinetics of the recarbonation reaction[40, 41, 47] together with well-established gas-solid contact reactor submodels[48] is needed to evaluate the extent of the impact of the recarbonator reactor in the scheme of Figure 1. This will contribute to the design of future pilots which will experimentally validate the improved CO_2 capture performance of the system studied in this work.

2. RECARBONATOR REACTOR MODELING

A bubbling fluidized bed reactor configuration was chosen for the recarbonator, as schematically outlined in Figures 1 and 2. The recarbonator reactor is regarded as an enlarged fluidized bed loop-seal that receives solids from the carbonator cyclone (see Figure 2). This loop-seal is fluidized by the CO_2 that reacts in the recarbonator and/or steam to facilitate fluidization, as will be discussed below. Since the use of CO_2 needs to be minimized because it comes from recycled flue gas released from the calciner, it is already clear that a substantial

fraction of the flow of reacting gas (CO_2) will disappear from the gas phase into the solid phase. At the same time, it is important to guarantee that the recarbonator reactor is continuously fluidized. This is achieved by ensuring that there is at all times an excess of gas to remain above the conditions of minimum fluidization. This fluidizing gas must also allow the necessary circulation of solids through the standpipes and loop-seals of the existing CaL system, which is known to be very sensitive to the fluidization conditions in the reactors and the loop-seals[49] and to external control of the solid circulation rates between the reactors[21].

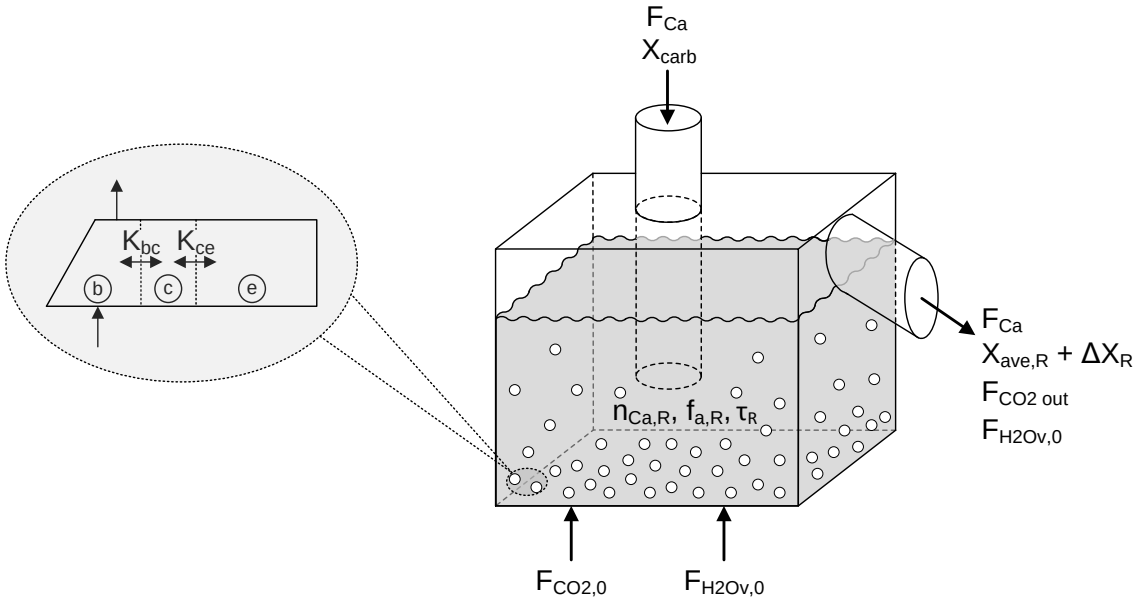

Figure 2. Scheme of the bubbling bed recarbonator with the main variables for reactor design. The bubble (b), cloud (c) and emulsion (e) regions are depicted on the left.

For the sake of simplicity, the recarbonator reactor of Figure 2 is assumed to have a constant cross-sectional area and all the CO_2 is injected through the bottom of the reactor (no secondary gas injections are considered). However, designs with a variable area to accommodate changes in the fluidizing gas flow rate due to the reaction of the CO_2 might be considered as feasible in the

future. For the same reasons, a further design decision affects the type of fluidizing gas selected for the recarbonator. If CO_2 is the only gas fed to the reactor, the rapid depletion of CO_2 and associated defluidization will take place in situations where there is an excess of active CaO arriving in the recarbonator reactor (this defluidization phenomenon has already been reported to occur[50] in the loop-seal of an oxy-fired facility fluidized with pure CO_2). To prevent these situations from occurring and to facilitate a minimum flow of fluidizing gas, a certain flow of steam is fed to the recarbonator. The steam may also help to enhance the recarbonation reaction, as the positive effect of steam on the diffusionally controlled stage of the carbonation of CaO has been reported by several authors[51, 52]. However, even when steam is used as an auxiliary fluidizing gas, a major fraction of the CO_2 fed through the bottom of the reactor ($F_{CO2,0}$) will disappear from the gas. This is schematically represented in Figure 2 and must be taken into account when modeling the gas-solid contact in the bubbling fluidized bed reactor.

In order to assess the effectiveness of the gas-solid contact in the recarbonator reactor, the model proposed by Kunii and Levenspiel[48] for bubbling beds of fine particles has been used in this work. The KL model postulates the existence of a bubble (b), cloud (c) and emulsion (e) phase (see Figure 2), and assumes spherical bubbles of a constant size, which rise faster than the gas that passes through the emulsion. Therefore, almost all the gas moving through the bed of solids is located in the bubble phase whereas the upflow of gas through the cloud and emulsion regions is small. The cloud and the emulsion are the dense regions and are considered to be at close to minimum fluidizing conditions. Besides, there are mass transfer phenomena between the bubble and the cloud and between the cloud and the emulsion, which can be quantified by means of the gas interchange rate coefficients defined by Kunii and Levenspiel (K_{bc} and K_{ce}

respectively). The existence of these three separate regions introduces diffusion resistances to the progression of the recarbonation reaction.

In the model described in this work the recarbonation reaction has been limited to the cloud and the emulsion regions, where most of the solids are located. Therefore, the contribution of the bubble phase has been neglected. The mass balances of the three regions included within the bubbling bed reactor have been performed, using the notation in Figure 2. When modeling the gas phase, the reduction in the CO_2 flow rate along the height of the reactor is taken into account by dividing the reactor into a series of reactor elements in the axial direction, considering a plug flow pattern in the bubble phase. In each of these elements the change in the gas volume is moderate and all bubble properties can be estimated as a constant value. With this procedure, the calculated outputs of each element (bubble density, bed porosity, gas and bubble velocities, molar flow and molar fraction of CO_2) are the input parameters for the subsequent element. On the other hand, when modeling the solid phase, the assumption in the KL model of an instant and perfect mixing of solids is retained for the recarbonator reactor. Therefore, in any of the volume elements considered axially for the gas phase, the properties of the solids are identical and equal to the properties of the solids at the exit of the reactor.

If the axial bed height is divided into Z volume elements the formulation of the KL model requires the establishment of mass balances for the bubble, cloud and emulsion regions depicted in Figure 2 for any element i (between 1 and Z). This gives Eqs. (1), (2) and (3), respectively:

$$-u_{b,i}\frac{dC_{b,i}}{dz} = K_{bc}\left(C_{b,i} - C_{c,i}\right) \quad (1)$$

$$K_{bc}\left(C_{b,i} - C_{c,i}\right) = a_{1,i}\alpha_{c,i}\left(C_{c,i} - C_{eq}\right) + K_{ce}\left(C_{c,i} - C_{e,i}\right) \quad (2)$$

$$K_{ce}\left(C_{c,i} - C_{e,i}\right) = a_{1,i}\alpha_{e,i}\left(C_{e,i} - C_{eq}\right) \quad (3)$$

where $u_{b,i}$ is the bubble rise velocity in the element i; $C_{b,i}$, $C_{c,i}$ and $C_{e,i}$ stand for the CO_2 molar concentrations in the bubble, cloud and emulsion regions, respectively, of the element i in the recarbonator and C_{eq} is the CO_2 molar concentration at equilibrium conditions. $a_{1,i}$ is derived from the kinetics of the recarbonation reaction, which will be discussed below.

In addition, $\alpha_{c,i}$ and $\alpha_{e,i}$ represent the fractions of solids that are present in the cloud and the emulsion regions, respectively, for each element i. They can be calculated from the parameters γ_c and $\gamma_{e,i}$ defined by Kunii and Levenspiel[48] as the volume of solids dispersed in the cloud and the emulsion regions, respectively, per volume of bubble:

$$\alpha_{c,i} = \frac{\gamma_c}{\gamma_c + \gamma_{e,i}} \quad (4)$$

$$\alpha_{e,i} = \frac{\gamma_{e,i}}{\gamma_c + \gamma_{e,i}} \quad (5)$$

The bubble fraction of the bed in the element i, δ_i, is required to obtain the $\gamma_{e,i}$ value[48]. The δ_i is calculated from the ratio between the superficial gas velocity and the velocity of the rising bubbles in the element when the minimum fluidization velocity is negligible with respect to the superficial gas velocity[48]. The velocity of the bubbles in a bubbling fluidized bed is a function of

the superficial gas velocity, the minimum fluidization velocity and the rise velocity of an isolated bubble, and is here calculated for each element by means of the expressions proposed by Davidson and Harrison[48, 53]. For this purpose, and for the sake of simplicity, the bubble diameter is assumed to be constant throughout the recarbonator, so that it is only the bubble fraction that diminishes along the reactor as CO_2 disappears from the gas phase to form $CaCO_3$.

It should also be noted that the porosity of the bed in every specific element i can be calculated when δ_i is known. This porosity results from the sum of the bubble fraction and the porosity of the dense regions, which are assumed to be at close to minimum fluidizing conditions[48]. Finally, the gas interchange coefficients K_{bc} and K_{be} are calculated by means of the expressions given by Kunii and Levenspiel[48]. These coefficients depend on the velocity and porosity at minimum fluidizing conditions, the bubble diameter and the molecular diffusion coefficient of the gas.

In order to extend the differential balances of Eqs. (1), (2) and (3) to an overall reactor element, it is assumed that the gas in the bubble phase can be described by means of a plug flow model (PFR). By combining the previous expressions and the PFR equations of a system with a constant volume, the CO_2 concentration in the bubble phase can be obtained for each element i as a function of the height along the element (z_i):

$$C_{b,i} = \frac{1}{1 - a_{2,i}}\left[\left(\left(1 - a_{2,i}\right)C_{b\ in,i} - a_{3,i}\right)e^{-\frac{K_{bc}\left(1-a_{2,i}\right)}{u_{b,i}}z_i} + a_{3,i}\right] \qquad (6)$$

In the above equation $a_{2,i}$ and $a_{3,i}$ are constants in each volume element i. They result from the combination of several variables when writing the integral that leads to equation (6), and are given by Eqs. (7) and (8) respectively:

$$a_{2,i} = \frac{K_{bc}}{K_{bc} + a_{1,i}\alpha_{c,i} + \frac{K_{ce}a_{1,i}\alpha_{e,i}}{K_{ce} + a_{1,i}\alpha_{e,i}}} \tag{7}$$

$$a_{3,i} = \frac{a_{1,i}\alpha_{c,i}C_{eq} + \frac{K_{ce}a_{1,i}\alpha_{e,i}C_{eq}}{K_{ce} + a_{1,i}\alpha_{e,i}}}{K_{bc} + a_{1,i}\alpha_{c,i} + \frac{K_{ce}a_{1,i}\alpha_{e,i}}{K_{ce} + a_{1,i}\alpha_{e,i}}} \tag{8}$$

Additionally, the CO_2 concentration in the cloud and the emulsion regions of any reactor element i can be obtained at any height by the expressions shown below, which are derived from combining Eqs. (2) and (3):

$$C_{c,i} = a_{2,i}C_{b,i} + a_{3,i} \tag{9}$$

$$C_{e,i} = \frac{K_{ce}}{K_{ce} + a_{1,i}\alpha_{e,i}}C_{c,i} + \frac{a_{1,i}\alpha_{e,i}C_{eq}}{K_{ce} + a_{1,i}\alpha_{e,i}} \tag{10}$$

Once the CO_2 concentration in the bubble phase at the exit of the element i is known, its gas conversion ($X_{CO2,i}$) can be calculated by means of Eq. (11) since the volume of gas remains virtually constant inside the reactor element:

$$X_{CO2,i} = \frac{C_{b\ in,i} - C_{b\ out,i}}{C_{b\ in,i}} \tag{11}$$

The value of $X_{CO2,i}$ obtained allows the moles of CO_2 that have reacted inside the element i to be calculated and hence, the number of moles of CO_2 that leave the element i and enter the element i+1. This value is also used to estimate the new operating parameters that will be used for the element i+1, i.e. the inlet concentration of CO_2, the bubble and gas velocities, the bubble density and the bed porosity in this reactor element. Finally, the gas conversion attained inside the overall reactor due to recarbonation and calculated by means of the gas balance ($X_{CO2,GB}$) is:

$$X_{CO2,GB} = \frac{F_{CO2\ in,1} - F_{CO2\ out,Z}}{F_{CO2\ in,1}} \quad (12)$$

where $F_{CO2\ out,Z}$ is the molar flow of CO_2 that leaves the recarbonator and $F_{CO2\ in,1}$ represents the CO_2 that enters the first reactor element.

In the previous equations (2), (3), (7), (8) and (10) the term $a_{1,i}$ contains the information relating to the kinetics of recarbonation at particle level. The investigation of the kinetics of the carbonation reaction has been the subject of many studies[4, 43, 54-57]. Nevertheless, very little quantitative information has been reported in relation to recarbonation conditions (very high partial pressures of CO_2 and temperatures over 750ºC) as these are unusual in carbonator reactors (partial pressures of CO_2 well below 0.1 atm and temperatures of around 650ºC). However, recent thermogravimetric studies by our group published elsewhere[47] have demonstrated that the kinetic parameters (pre-exponential factor and activation energy) derived for the carbonation conditions are still valid for the recarbonation conditions. A typical example of such an experiment, which represents a conversion vs time curve of a calcined sample subjected to carbonation and recarbonation, is presented in Figure 3.

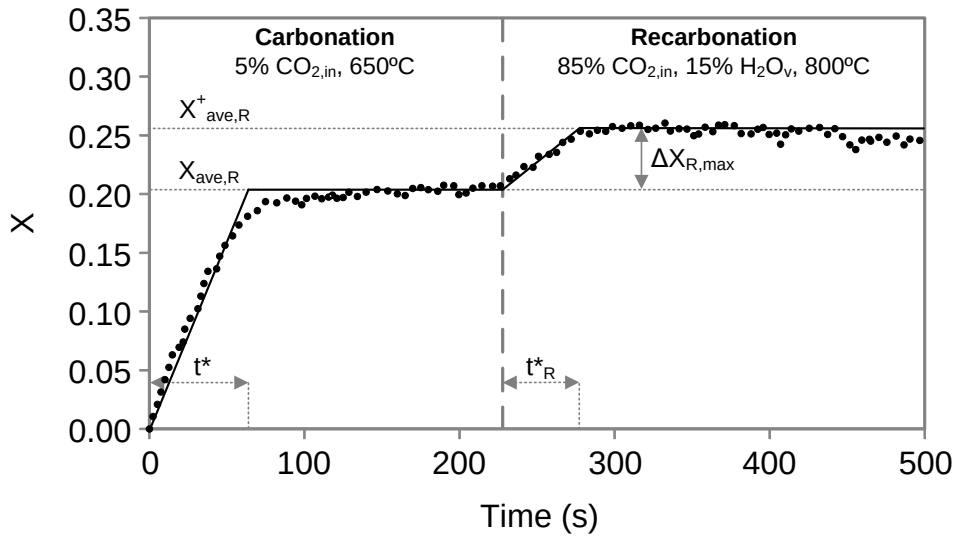

Figure 3. Example of a typical conversion vs time curve during carbonation and recarbonation stages.

Since the particles arriving at the carbonator are perfectly mixed and contain a wide distribution of particles with a different cycle number, we have used the subscript "ave" to refer to the average particle properties, although in this particular example of Figure 3, these average properties correspond to two cycles of carbonation-recarbonation-calcination of a previously deactivated sorbent (after 15 standard carbonation-calcination cycles)[47]. Furthermore, to distinguish from previous definitions of the CO_2 carrying capacity of the sorbent, we have referred to the average CO_2 carrying capacity of the particles arriving from the calciner to the carbonator in the system of Figure 1 as $X_{ave,R}$. Figure 3 indicates that in the carbonator reactor these particles are subjected to a carbonation step where they undergo a maximum carbonate conversion equal to $X_{ave,R}$ if they have a residence time in the carbonator longer than the characteristic time t*. These particles carbonated to their maximum CO_2 carrying capacity are

unable to react with CO_2 under carbonation conditions (see the negligible progress in conversion between 80 and 220 s in Figure 3). However, when they are subjected to the conditions in the recarbonator reactor (at 800ºC and 85%v CO_2 in steam in the example of Figure 3) a new reaction stage is initiated. As a result, the particles increase their carbonate content from $X_{ave,R}$ to a higher value, which can be represented as $X^{+}_{ave,R}=X_{ave,R}+\Delta X_{R,max}$, if the recarbonation is allowed to progress until t^*_R.

In a recent paper focused on the kinetics of these reactions we observed[47] that the recarbonation process goes through a fast period where the reaction rate is constant from the onset of the recarbonation period at $X_{ave,R}$ until the solids reach a conversion of $X^{+}_{ave,R}$. Hereafter the reaction rate is zero. In these conditions and by analogy with the approach adopted for the carbonator reactor models described elsewhere[20, 58] the reaction rate in the recarbonator reactor is modeled using Eq. (13):

$$\frac{dX}{dt} = k_{s,R} X_{ave,R}\left(\overline{\nu - \nu_{eq}}\right) \quad \text{for } X_{ave,R}<X<X^{+}_{ave,R} \tag{13a}$$

$$\frac{dX}{dt} = 0 \quad \text{for } X=X^{+}_{ave,R} \tag{13b}$$

where $k_{s,R}$ is the recarbonation reaction rate constant, ν is the volume fraction of CO_2 in the gas phase and ν_{eq} is the volume fraction of CO_2 at equilibrium conditions.

The time required for the solids to attain maximum conversion after recarbonation ($X^{+}_{ave,R}$) in the reactor, t^*_R, can also be obtained from the maximum increase in the carbonate content of the particles within the recarbonator divided by the recarbonation reaction rate:

$$t_R^* = \frac{\Delta X_{R,max}}{dX/dt} \quad (14)$$

Furthermore, when using equation (13a) to write the reaction term of the mass balances represented by equations (2) and (3) the kinetic term $a_{1,i}$ can be derived as follows:

$$a_{1,i} = \frac{k_{s,R} X_{ave,R}\, \rho_s (1-\epsilon_i) f_{a,R} f_{Ca,R\,w}}{\delta_i \rho_{m,g} M_s} \quad (15)$$

where ρ_s is the solids density, ϵ_i is the bed porosity in the reactor element i, $f_{a,R}$ is the fraction of solids that are active for the recarbonation reaction, $f_{Ca,R\,w}$ is the mass fraction of calcium that is involved in the recarbonation process (the inerts are subtracted), $\rho_{m,g}$ is the molar density of the gas and M_s is the molecular weight of the calcium solids.

It must be pointed out here that Figure 3 and the choice of the kinetic constant $k_{s,R}$ for the recarbonation period is consistent with the experimental information available from TG tests reported elsewhere[41, 47]. From the recent experiments carried out by Grasa et al.[47] the apparent kinetic constant for the recarbonation ($k_{s,R}$) is 0.004 s^{-1} (vs k_S=0.33 s^{-1} obtained for the carbonation reaction at 650ºC[20]), and this is the value used in this work for the simulation studies. It should be noted that this is a conservative $k_{s,R}$, since the presence of steam in the reaction atmosphere is known to lead to higher values of the kinetic constant as a result of the enhancement in the recarbonation reaction. As Figure 3 indicates, despite the kinetic constant during recarbonation being two orders of magnitude slower than the constant during fast carbonation, a substantial rate of recarbonation reaction can be achieved thanks to the increased

CO_2 concentration in the recarbonator reactor. This is essentially the fundamental idea behind the proposed reactivation process, as particles are forced to regain a higher carbonation conversion (a synonym for CO_2 carrying capacity) as they go through the recarbonator reactor so that the subsequent loss in activity during the next calcination cycle allows higher levels of CO_2 carrying capacities to be sustained[41, 47].

Finally, in the KL model equations for the recarbonator reactor it is implicitly assumed (through the term $f_{a,R}$ in equation (15)) that an average fraction of active solids exists in the solid phase within the bed, which is the only fraction of solids that reacts with the gas phase. Indeed, the fraction of particles that have been in the recarbonator for a period longer than t^*_R have increased their carbonate content by $\Delta X_{R,max}$ and they are no longer able to react with CO_2 (see equation (13b)). Only the fraction of particles which have remained in the reactor for a period shorter than t^*_R is able to recarbonate, and it represents the active fraction of particles:

$$f_{a,R} = 1 - e^{-t^*_R/\tau_R} \qquad (16)$$

This is an analogous procedure to that of the carbonator reactor described elsewhere[58]. It takes into account the ideal residence time distribution of the particles entering a well-mixed fluidized bed[59], which has been proven to be successful for modeling lab-scale[19, 20] and large-scale pilot data[21] of fluidized bed carbonator reactors. The mean residence time of the solids inside the recarbonator, τ_R, can be obtained as the ratio between the number of Ca moles inside the recarbonator ($n_{Ca,R}$) and the flow of Ca moles (F_{Ca}):

$$\tau_R = \frac{n_{Ca,R}}{F_{Ca}} \quad (17)$$

The calculation of the increase in calcium carbonate moles circulating between the carbonator and the calciner due to recarbonation ($F_{Ca}\Delta X_R$) requires the definition of the ΔX_R term, which is the average of the conversion achieved by the particles with a residence time below the threshold for achieving the maximum conversion and those that have reached the maximum conversion $X^{+}_{ave,R}$ (or the extra carbonation conversion $\Delta X_{R,max}$):

$$\Delta X_R = f_{a,R}\Delta X_{R,t<t_R^*} + (1 - f_{a,R})\Delta X_{R,t>t_R^*} \quad (18)$$

The two addends of the previous equation can be obtained by following the same procedure as that described by Alonso et al.[58] for a carbonator reactor, taking into account the residence time distribution of the particles inside perfectly mixed reactors. Rearrangement of these expressions leads to the carbonate conversion of the particles inside the recarbonator:

$$\Delta X_R = \Delta X_{R,max}\frac{\tau_R}{t_R^*}\left(1 - e^{-t_R^*/\tau_R}\right) = -\frac{\Delta X_{R,max}\, f_{a,R}}{\ln(1 - f_{a,R})} \quad (19)$$

The CO_2 mass balance then gives the following conversion in the gas phase:

$$X_{CO2} = \frac{F_{Ca}}{F_{CO2\ in,1}}\Delta X_R \quad (20)$$

On the other hand, the calculation of t^*_R for each element (Eq. (14)), requires the definition of the average CO_2 volume fraction in the reacting phases (cloud and emulsion) to obtain the value of dX/dt (Eq. (13a)). Since this is also changing in the Z axial reactor elements adopted for the resolution of the model, it has to be estimated by taking into account these plug flow reactors for the gas, while maintaining a perfect and instant mixing of solids throughout the bed. Thus:

$$k\tau_i = \frac{\rho_{m,g}\, \nu_{b\ in,i} X_{CO2,i}}{\left(\overline{\nu_c - \nu_{eq}}\right)_i \alpha_{c,i} + \left(\overline{\nu_e - \nu_{eq}}\right)_i \alpha_{e,i}} \tag{21}$$

$$k\tau_i = \frac{\rho_{m,g}}{a_{4,i}} \ln\left(\frac{a_{4,i} C_{b\ in,i} + a_{5,i}}{a_{4,i} C_{b\ out,i} + a_{5,i}}\right) \tag{22}$$

where $\nu_{b\ in,i}$ is the CO_2 volume fraction in the bubble phase at the inlet of the element i, ν_c and ν_e are the CO_2 volume fractions in the cloud and the emulsion, respectively, and $a_{4,i}$ and $a_{5,i}$ are constants and can be calculated by means of expressions (23) and (24):

$$a_{4,i} = \alpha_{c,i} a_{2,i} + \frac{\alpha_{e,i} K_{ce} a_{2,i}}{K_{ce} + a_{1,i} \alpha_{e,i}} \tag{23}$$

$$a_{5,i} = \alpha_{c,i} a_{3,i} + \frac{\alpha_{e,i} K_{ce} a_{3,i} + a_{1,i} \alpha_{e,i}^2 C_{eq}}{K_{ce} + a_{1,i} \alpha_{e,i}} - C_{eq}\left(\alpha_{c,i} + \alpha_{e,i}\right) \tag{24}$$

Finally, the combination of Eqs. (21) and (22) gives the average of the difference between the CO_2 concentration in both the cloud and the emulsion regions and that at equilibrium conditions in a specific reactor element:

$$\left(\overline{\nu_c - \nu_{eq}}\right)_i \alpha_{c,i} + \left(\overline{\nu_e - \nu_{eq}}\right)_i \alpha_{e,i} = \frac{a_{4,i} \nu_{b\ in,i} X_{CO2,i}}{\ln\left(\frac{a_{4,i} C_{b\ in,i} + a_{5,i}}{a_{4,i} C_{b\ out,i} + a_{5,i}}\right)} \quad (25)$$

The solution of the model applied above allows the calculation of the gain in the carbonate conversion of the particles inside the recarbonator reactor, the efficiency of the reactor (taken to be the ratio between $\Delta X_R/\Delta X_{R,max}$) and the conversion of the gas (X_{CO2}). It should be noted that the carbonation conversion of the solids arriving at the reactor (X_{carb}) is not equal to $X_{ave,R}$ but slightly lower under the typical operating conditions of the carbonator. This means that particles arriving at the recarbonator first have to be carbonated up to $X_{ave,R}$ before the recarbonation process can take place. This carbonation process is assumed here to be virtually instantaneous, as the kinetic constant of the carbonation is much higher than that of the recarbonation reaction and the recarbonator is also operating at a high temperature and with a high concentration of CO_2.

As discussed by Arias et al.[41] the fraction of unconverted active CaO ($X_{ave,R}$-X_{carb}) arriving in the recarbonator has to be kept to a minimum because the carbonation of this CaO translates into a higher demand for CO_2 in the recarbonator (and a higher associated cost). However, this fraction of active CaO is beneficial in that it increases the temperature of the solids in the recarbonator reactor thanks to the exothermic carbonation reactions taking place in the atmosphere of concentrated CO_2. In this work we consider that the CO_2 available for the actual recarbonation of the particles is the CO_2 entering the reactor minus the CO_2 used for this instantaneous carbonation. Therefore, this is the gas flow that will be considered to be involved in the recarbonation process and that will be used to calculate the properties of the bed, such as the bubbles velocity and the bubble density in the reactor. This approach is supported by

assuming that the particles inside the recarbonator are well mixed and the solids which are constantly arriving at the recarbonator at X_{carb} are rapidly distributed throughout the reactor and react instantaneously to reach $X_{ave,R}$.

The recarbonator model is solved by following an iterative procedure (see Figure 4) that was programmed using Matlab. Once all the inlet parameters of the model are fixed, the procedure begins with the calculation of the CO_2 used to carbonate the particles from X_{carb} up to $X_{ave,R}$ ($F_{CO2,carb}$). Then, the CO_2 consumed in this process is subtracted from the total CO_2 fed to the reactor ($F_{CO2,0}$) and the inlet flows and parameters of the first reactor element are calculated, as outlined in Figure 4. Assuming a first tentative value of $f_{a,R}$, the conversion of the gas can be calculated by using the expressions obtained through the solids balance (Eq.(20)) and the gas balance (Eq.(12)). To obtain the gas conversion from the gas balance it is necessary to solve all the Z reactor elements of the recarbonator (100 volume elements have been used in the simulations), where the outlet parameters of an element i are the inlet variables for the next element i+1 while identical solid properties are maintained in all the elements. Finally, the gas conversions given by Eqs. (20) and (12) are compared. If the difference between them is found to be less than the defined tolerance value, the iterative process based on $f_{a,R}$ ends, leading to the value of the conversion of the gas and the efficiency of the recarbonator. Nevertheless, if the difference is higher than the tolerance value, the process is repeated again using a new value of $f_{a,R}$ until a solution is found.

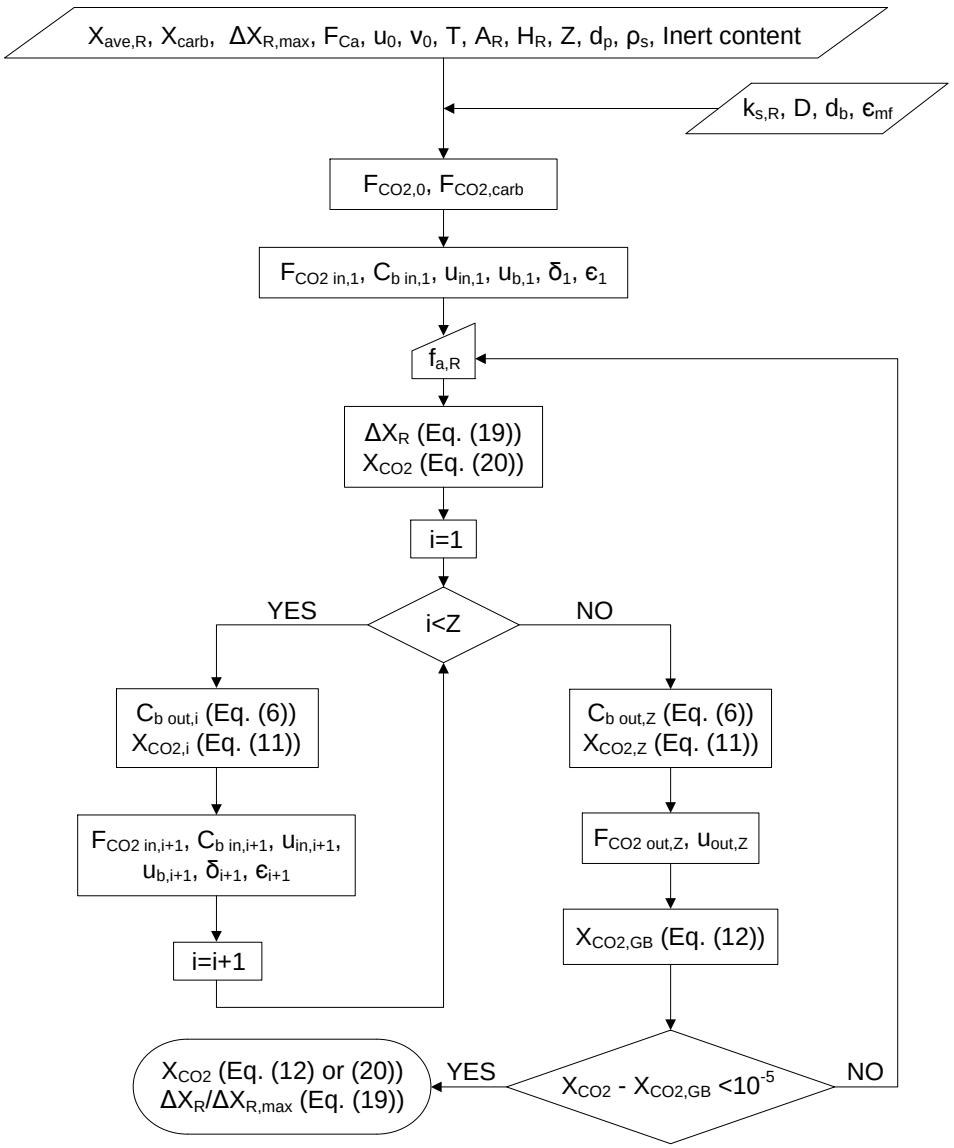

Figure 4. Scheme of the calculation procedure for the proposed model.

In this way, the model is able to calculate for a given set of reaction conditions (inlet gas concentration and reactor temperature), inlet mass and gas flows and reference reactor volume, the average recarbonation conversion achieved by the solids at the exit of the reactor, and in turn the efficiency of the recarbonation reaction, the gas conversion and the gas flow rates and compositions at the exit of the reactor. Consequently, the model can be used as a simulation tool

to analyze the key design parameters of the reactor in order to achieve the targeted level of recarbonation efficiency.

3. SIMULATION OF THE RECARBONATOR REACTOR

In the following paragraphs we report a design exercise to illustrate how to determine the volume of the recarbonator reactor, using the solution procedure described above for the reference set of operating conditions and model parameters compiled in Table 1. One of the problems in selecting the reference conditions for the reactor is that, as indicated in Figure 1, the recarbonator reactor is a part of a three reactor CaL system, so that the input flows for the recarbonator reactor are the output flows of the carbonator reactor and the output flows in the recarbonator reactor also have an impact on the performance of the calciner and carbonator reactors. Therefore, for the sake of clarity in the present simulation exercise, we have chosen a set of boundary conditions and input flows for the recarbonator reactor that are considered constant and independent of the carbonator and calciner performances. The calciner is assumed to operate with 100% calcination efficiency with respect to the $CaCO_3$ flow entering the calciner and the carbonator is assumed to operate with 85% carbonation efficiency with respect to the flow of active CaO entering the carbonator. It is beyond the scope of this work to analyze in detail how these efficiencies can be obtained in practice. However, these can be considered reasonable assumptions in light of the experimental results obtained from pilots of different scale[16-23] and carbonator model predictions[12, 20, 21, 58, 60] for reactors operating with sufficient solid residence times and active flows of solids.

Table 1. Input parameters for the recarbonator model.

Ref. operating variable	**Value**
$X_{ave,R}$	0.20
X_{carb}	0.17
$\Delta X_{R,max}$	0.03
F_{Ca} (mol/s)	10000
$F_{CO2,0}$ (mol/s)	700
T (ºC)	800
ν_0	0.85
d_p (μm)	100
ρ_s(kg/m^3)	2000
Inerts (%w)	30
Model Parameters	**Value**
$k_{s,R}$ (s^{-1})	0.004
D (m^2/s)	1.98*10^{-4}
d_b (m)	0.05
ϵ_{mf}	0.43
K_{bc} (s^{-1})	6.47
K_{ce} (s^{-1})	3.94

Also indicated in Table 1 is the fact that we are assuming an average carrying capacity of the solids entering the carbonator and recarbonator reactors of $X_{ave,R}$=0.20. This level of activity is made possible in the system of Figure 1 by the combined effect of a certain limestone make-up flow to the calciner and the positive effect of the recarbonation conversion ΔX_R that will be achieved in the recarbonator reactor. In principle, we fix this value of $X_{ave,R}$=0.20 in Table 1 as an input parameter, although it is at the same time a design target for the recarbonator reactor to reach this average CO_2 carrying capacity by minimizing the make-up flow of limestone to the calciner. This means that if the recarbonator reactor is ineffective, a large make-up flow of limestone will be required to reach the CO_2 carrying capacity of 0.20 adopted as a reference. In contrast, if the recarbonator reactor achieves a ΔX_R of around 0.02 it has been experimentally demonstrated[41, 42, 47] that a residual conversion of lime of 0.16-0.17 can be achieved. In that case a very small make-up flow of limestone will be required to achieve the targeted $X_{ave,R}$=0.20. The

addition of a small make-up flow of limestone will always be necessary to purge ashes and $CaSO_4$ and to maintain a reasonable buildup of inert materials in the system[26]. Earlier works describing the CaL system mass balances[57, 60-63] provide detailed methods for quantifying the make-up flow requirements of limestone in order to sustain a certain level of average CO_2 carrying capacity as a function of the limestone deactivation parameters and the ash and sulfur present in the fuel burned in the calciner.

The input of solids into the reactor (F_{Ca} in Figure 2) is assumed to be 10000 mol/s as a reference and this solids stream is assumed to contain a typical 30% of inert material (ash and $CaSO_4$ as discussed by Diego et al.[26]). The carbonate conversion of this calcium flow to the recarbonator is X_{carb}=0.17 (because of the 85% carbonation efficiency assumed in the carbonator). The resulting CO_2 capture rate in the carbonator of 1700 mol/s would correspond to the CO_2 captured from a power plant of about 1000 MW_{th}, equipped with a carbonator reactor of about 200 m^2 of cross-sectional area operating at around 5 m/s. These are all typical targets for large- scale carbonator reactors[12, 16-23, 58, 60], comparable in size to the commercial circulating fluidized bed combustors with a similar thermal input. The purpose of these assumptions about the carbonator dimensions is to be able to compare the dimensions of the new recarbonator reactor against large scale reactors in "standard" Calcium Looping CO_2 capture systems. Additionally, the $\Delta X_{R,max}$ of the lime particles is taken to be 0.03, which is a conservative value according to the experimental data reported elsewhere[41, 47]. The values assumed for $X_{ave,R}$ and $\Delta X_{R,max}$ lead to a maximum sorbent conversion at recarbonator outlet $X^{+}_{ave,R}$=0.23.

Finally, the gas input to the recarbonator reactor is assumed to have 85%v of CO_2 and 15%v of steam, while the reaction temperature is taken to be 800ºC, since these operating conditions have been proven to be adequate for fast recarbonation kinetics[47]. The CO_2 molar flow rate to the recarbonator is set in the reference case at 700 mol/s, which leaves an excess molar flow of CO_2 for the recarbonation once the particles have been carbonated up to $X_{ave,R}$ (this process consumes 300 mol CO_2/s). For the KL model parameters, the particles are assumed to have an average size of 100 μm and a density of 2000 kg/m^3, which are typical values in CaL systems, and the bubble diameter is assumed to be 0.05 m. The recarbonation rate constant is taken as 0.004 s^{-1} on the basis of the discussion in the previous section and the experimental data obtained by Grasa et al.[47].

Figure 5 presents a first set of model predictions for the reference case of Table 1, in which the efficiency of the recarbonator reactor (ratio $\Delta X_R/\Delta X_{R,max}$) is calculated as a function of the reactor volume. Four different curves have been generated for different expanded reactor heights (0.5, 1, 2 and 3 m). This means that, for a given reactor volume, four different cross sections of the reactor and gas velocities are plotted in the figure, since the total molar flow of gas has been fixed in the reference Table 1. Furthermore, in each of the curves of Figure 5, the changes in reactor volume translate into proportional changes in the cross-sectional area and superficial gas velocity. The specific conditions in each case (superficial gas velocity, gas conversion) result in a different bed porosity, which allows calculating the inventory of solids within the recarbonator for a given reactor geometry.

The figure shows the expected trend of an initial sharp increase in reactor efficiency as the volume of the reactor (and associated solids residence time, τ_R) increases. For larger recarbonator volumes the increase in reactor efficiency is more moderate because the total consumption of CO_2 moles is high, so that the CO_2 molar concentration is closer to equilibrium and the solids conversion approaches its maximum ($\Delta X_{R,max}$=0.03 as indicated in Table 1). When the four curves of Figure 5 are compared, it can be seen that shallower reactors are more efficient than deep beds for smaller reactor volumes, whilst the opposite happens at higher reactor volumes.

This trend can be explained on the basis of the two effects described next. When the superficial gas velocity is lower (this is the case of shallower reactors, since the inlet molar flow of gas is constant), the expansion of the bed is lower, so that for a given reactor volume, the mean residence time of the particles inside the recarbonator and thus, the reactor efficiency, are higher. This effect dominates on the left hand side of Figure 5. Nevertheless, this expected trend is not repeated for large reactor volumes, as another effect controls in the right hand side of the figure. For a given height of the expanded bed, if the inlet molar flow of gas is constant, an increase in the recarbonator volume translates into a decrease in the superficial gas velocity. As a consequence, the solids tend to concentrate in the emulsion region rather than in the cloud region (see the expressions for γ_e and γ_c in the KL model[48]). It is known that the diffusion of CO_2 to the emulsion phase suffers more hindrance and this region tends to get closer to the CO_2 concentration of the equilibrium, as a result of which the recarbonation reaction rate is slowed down. This effect is more pronounced at lower gas velocities, that is, for higher reactor volumes and shallower recarbonator reactors, and it explains the change in the tendency observed in Figure 5. A limit has been marked in Figure 5, which is represented by the dotted line on the left

hand side of the figure corresponding to a maximum fluidizing velocity of 2 m/s. The lower velocity limit is imposed by the minimum fluidization velocity, u_{mf}. However, this is not shown in Figure 5 because none of the cases represented in this figure lead to velocities below u_{mf}.

These results seem to indicate that a target of very high recarbonator efficiencies (ratios $\Delta X_R/\Delta X_{R,max}$ of over 0.9) may not be realistic because they would entail very large reactor volumes and/or very large cross sections. For comparison purposes the cross-section of the carbonator and calciner in Figure 1 for this reference case will be of the order of 200 m^2 (which is in turn comparable to the cross-section of a circulating fluidized bed combustor in a power plant of 1000 MW_{th}, used as a reference for the data in Table 1). The ΔX_R targeted in the recarbonator is 0.02 ($\Delta X_R/\Delta X_{R,max}$=0.66), as was explained above. Therefore, reactor volumes of around 150-200 m^3 would be required depending on the expanded bed height. It is necessary to reach a compromise between sufficiently high reactor efficiencies during recarbonation and reasonable recarbonator dimensions. For this purpose, a recarbonator with a cross-section of between 80 and 100 m^2 (approx. 40 or 50% respectively of that of the carbonator) and 2 m of expanded bed height has been selected as a reasonable trade-off.

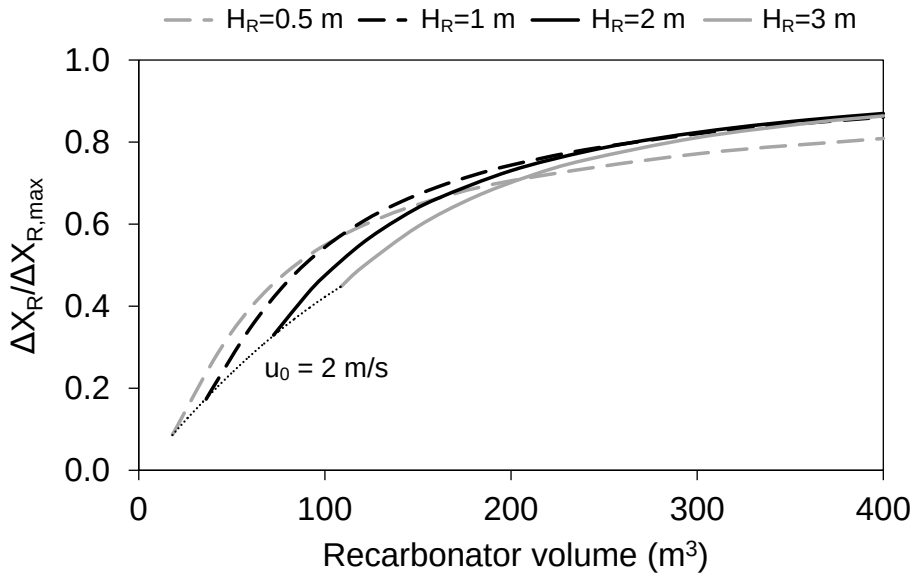

Figure 5. Efficiency of the recarbonator reactor ($\Delta X_R/\Delta X_{R,max}$) as a function of reactor volume, using different expanded reactor heights. Operating conditions as in Table 1.

The effect of the superficial gas velocity at the entrance to the recarbonator reactor for a given set of reactor dimensions (100 m^2 of cross-section and 2 m of expanded bed height as chosen above) is represented in Figure 6, for two operating temperatures (750ºC and 800ºC). In this case, the flow of solids entering the reactor is retained as in Table 1 but the gas flow rate is allowed to change, as indicated by the gas velocity at the entrance to the reactor. At very low gas velocities, the efficiency of the reactor deteriorates very rapidly in this example because the limiting factor hindering the reaction is the lack of CO_2 to sustain the fast carbonation stage (between X_{carb} and $X_{ave,R}$) and the recarbonation. In actual fact, the efficiency is zero if the inlet CO_2 molar flow is allowed to be exactly that required for instantaneous carbonation up to $X_{ave,R}$ plus the CO_2 associated to the equilibrium (gas velocity of around 0.3 m/s in Figure 6). The efficiency of the reactor reaches a maximum at around u_0=0.8 m/s (800ºC) and u_0=0.7 m/s (750ºC) (equivalent to $F_{CO2,0}$=770 mol/s and $F_{CO2,0}$=700 mol/s, respectively) and then drops

slightly as the excess CO_2 fed to the recarbonator expands the bubbling bed (leading to a reduction in the residence time of the solids as discussed above) without increasing the solids conversions. The excess CO_2 at the inlet also causes a drop in CO_2 conversion, X_{CO2}, calculated with equation (12) or (20) and also represented in Figure 6.

The efficiency in the conversion of CO_2 in the recarbonator reactor, X_{CO2}, needs to be maximized because this is a recycle flow that is obtained from the gas stream that leaves the calciner of Figure 1. However, the gas flow of CO_2 entering the recarbonator must be kept sufficiently high to maintain the high partial pressure of CO_2 required for fast recarbonation and intense fluidizing conditions so that it can serve as a loop-seal between the carbonator and calciner reactors. The shaded area in Figure 6 represents a reasonable compromise between a recarbonator efficiency of 0.60-0.70 (ΔX_R of around 0.02) and a X_{CO2} value of no less than 0.70 for an operation temperature in the recarbonator of 800ºC. The results show that an inlet gas velocity of around 0.6 m/s is enough to attain the targeted ΔX_R of 0.02 whilst maintaining at the same time a sufficiently high gas conversion (73%). This results in a mean residence time of the particles inside the recarbonator reactor of 167 s and a CO_2 molar flow of 251 mol/s available for recarbonation (after the particles have attained $X_{ave,R}$ and after the subtraction of the CO_2 moles associated to the equilibrium). At the temperature of operation chosen as a reference in Table 1 (800ºC), a minimum of 315 mol CO_2/s needs to be fed into the reactor to compensate for the total molar flow of CO_2 consumed in the reaction up to $X_{ave,R}$ plus the flow of CO_2 related to the equilibrium ($\nu_{CO2,eq}$=0.217)). If the recarbonator cross-section were 80 or 90 m^2, an inlet gas velocity of 0.9 and 0.7 m/s would be required, respectively, instead of 0.6 m/s, and the gas conversions would be lower (50 and 66% respectively). On the other hand, the less favorable

kinetics at 750ºC[47] leads to lower reactor efficiencies in this particular example and for this particular set of kinetic parameters ($k_{s,R}$ is taken to be 0.002 s^{-1} at 750ºC).

It should be highlighted that the total values of CO_2 consumption are only a small fraction (less than 10%) of the CO_2 generated in the calciner, which typically has a thermal input comparable to the power plant feeding flue gases to the carbonator of Figure 1[4, 7-9, 11, 13, 25] and therefore generates flows of CO_2 that are one order of magnitude higher. As for the steam requirements, they do not entail any additional penalty to the process since the recarbonator is directly fed using the gas stream that exits the calciner (prior to the condensation and purification step), which provides sufficient steam for recarbonation.

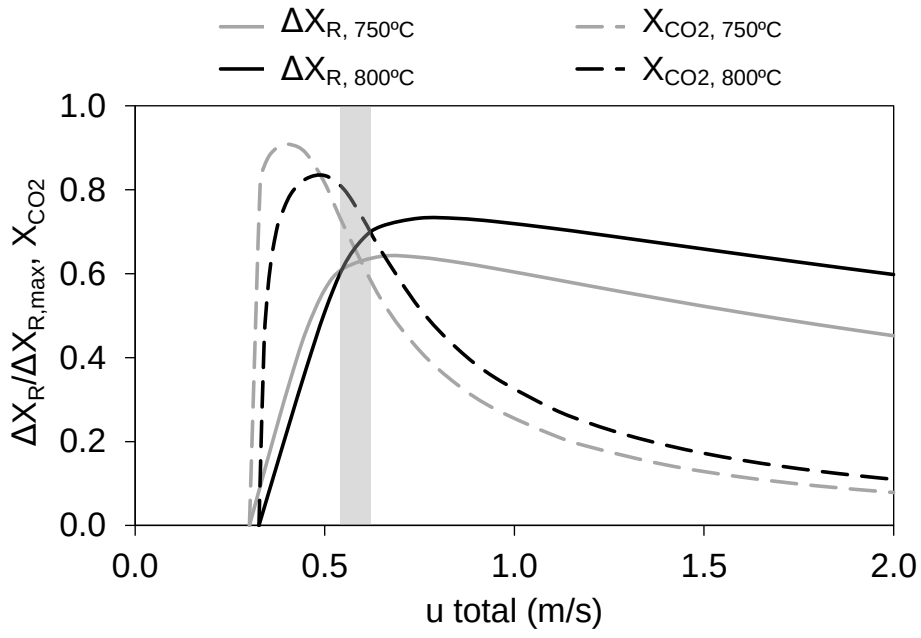

Figure 6. Efficiency of the recarbonator reactor ($\Delta X_R/\Delta X_{R,max}$) and gas conversion ($X_{CO2}$) as a function of the total inlet gas velocity at two operating temperatures (750 and 800ºC) for a

recarbonator of 100 m^2 and 2 m of expanded bed height. Solids flows and gas characteristics as in Table 1.

The previous design examples confirm that there are sufficiently wide design and operating windows to build and operate a recarbonator reactor aimed at the desired targets of sorbent recarbonation. There are however, still a number of uncertainties to be addressed, but these will be overcome as more data are obtained from the pilot testing campaigns in the 1.7MW_{th} pilot of La Pereda[21]. One such uncertainty is the extent of the impact of the recarbonator reactor temperature on the recarbonation conversions. The temperature chosen in this work as a reference (800ºC) is necessary to provide sufficiently fast recarbonation rates and reasonable recarbonator dimensions as pointed out above. However, this temperature is difficult to reach in practice when the inlet temperature of the solids coming from the carbonator is 650ºC and only around 5 net points of exothermic carbonation conversion (from X_{carb}=0.17 to $X_{ave,R}+\Delta X_R$=0.22) are available for reaction during recarbonation. An adiabatic heat balance to the reactor reveals that a temperature increase of only about 60-70ºC can be expected in the recarbonator in these conditions. If recarbonation were ineffective at a temperature between 700-750ºC because of the unfavorable kinetics[47], an additional means of increasing the temperature in the recarbonator reactor would be needed, such as an increase in the temperature of the carbonator (up to 700ºC the carbonator efficiency is still over 80% for typical coal flue gases), a parallel oxyfuel combustion of a small flow of fuel and O_2 fed to the recarbonator, or the preheating of the carbonated solids leaving the carbonator using a high-temperature flue gas[64]. The energy penalty associated to these processes in the overall system would be minimum, as all the heat provided in the recarbonator to increase the temperature of the solids would lead to a proportional decrease

in the heat requirements in the calciner. In fact, the recarbonation process should not entail a noticeable increase in the energy requirements of the calciner in the CaL system. This is because the additional heat demand in the calciner associated with the increase in the calcination of a solids stream with a higher carbonate content would be compensated for by the higher temperature of the solids arriving at the calciner of Figure 1 from the recarbonator.

A sensitivity analysis has been carried out to investigate the impact of the main model parameters on the calculated efficiency, $\Delta X_R/\Delta X_{R,max}$. Figure 7 depicts the influence that d_b, K_{bc}, K_{ce}, Υ_c and $k_{s,R}$ have on the the efficiency of the recarbonator when these parameters are altered between 50 and 150% with respect to the central values shown in Table 1. The solid flow and the gas properties correspond to those of Table 1, whereas the geometry of the recarbonator has been fixed at 100 m^2 and 2 m of expanded bed height, and the inlet gas velocity at 0.6 m/s.

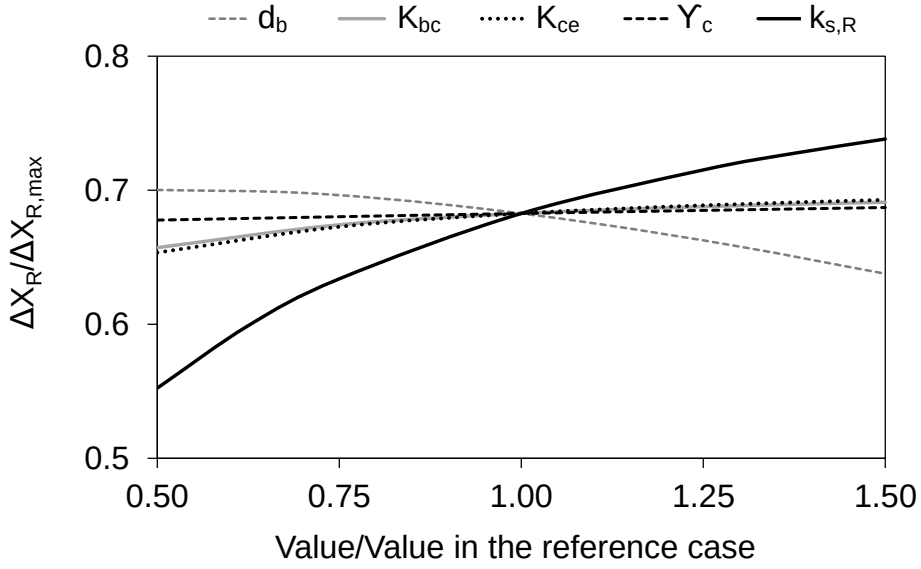

Figure 7. Sensitivity analysis of the effect of d_b, K_{bc}, K_{ce}, Υ_c and $k_{s,R}$ on recarbonation efficiency. Solid and gas properties as in Table 1. The inlet gas velocity is 0.6 m/s.

As can be seen in Figure 7, the bubble size has only a slight influence on the recarbonator effciency. It is known that when the bubble size decreases CO_2 transfer from the bubble to the cloud and subsequently to the emulsion is favored. However, the bed porosity also increases, and this translates into a reduction of the mean residence time of the particles inside the recarbonator. Nonetheless, these two effects compensate each other in the recarbonator reactor under these operating conditions, resulting in a virtually unchanged recarbonator efficiency (see Figure 7). It is important to note that the opposite happens when the bubble diameter increases. If the recarbonator efficiency were affected by an increase in the bubble size along the reactor, internals or some other device could be installed to reduce the size of the bubbles and boost the mass transfer of CO_2 to the emulsion phase. The effect of the interchange rate coefficients K_{bc} and K_{ce} has also been studied. It should be noted that these parameters are influenced by the bubble diameter, so that they have implicitly changed with d_b, but in that case the mean residence time has also altered due to changes in the bed porosity. When only K_{bc} and K_{ce} vary (τ_R remains virtually constant) it can be observed that the recarbonator efficiency is hardly affected. The same happens when Υ_c takes values ranging from 50 to 150% of that of the reference case: there is only a negligible effect on the efficiency of the recarbonator. The influence of Υ_e has not been considered in this study because it depends on the bed porosity, which changes in each case. Besides, it is directly related to Υ_c, so that a change in Υ_c also produces a change in Υ_e.

Finally, the kinetic constant is the parameter that most influences the recarbonator performance, although its effect is also limited. As expected, higher values of $k_{s,R}$ result in higher recarbonation efficiencies. But, as the final solids conversion is also affected by the equilibrium,

the available molar flow of CO_2 for recarbonation and the mean solids residence time inside the recarbonator, the efficiency increase is limited. Nevertheless, the $\Delta X_R/ \Delta X_{R,max}$ ratio diminishes more sharply for the lowest values of $k_{s,R}$, as can be seen from Figure 7.

The results presented in Figures 5-7 indicate that there are reasonable design and operating windows for the recarbonator reactor to achieve the desired targets of increased carbonation conversion. More importantly, this increase in conversion could allow the process to proceed with a significantly lower make-up flow for a specific target of average CO_2 carrying capacity and CO_2 capture efficiency, and lead to a reduction in the operational costs associated to CaL technology. Work is in progress to retrofit the La Pereda 1.7 MW_{th} pilot[21] with a recarbonator reactor to experimentally test this process variant of the postcombustion Calcium Looping system and exploit its advantages. The reactor model described in this paper will serve as a tool for interpreting and scaling up results obtained from the pilot.

4. CONCLUSIONS

A mathematical model of a fluidized bed recarbonator reactor, the aim of which is to increase the average CO_2 carrying capacity of the sorbent in a Calcium Looping CO_2 capture system, can be solved by integrating into the KL model the kinetic information available for the carbonation and the recarbonation reactions. The simulations of a large-scale system have identified reasonable operating windows where adequate recarbonation conversions (of the order of a 0.02 net increase in CaO conversion to $CaCO_3$) can be achieved and hence, average CO_2 carrying capacities close to 0.20 can be sustained. The solution of the recarbonator model indicates that average residence times from 100 to 170 s are sufficient for this purpose. An expanded bed

height of 2 m, a cross-sectional area of between 80 and 100 m^2 and an inlet gas velocity ranging from 0.6 and 0.9 m/s are required. These dimensions and conditions could be achieved with the loop-seals used to connect the carbonator and calciner reactors in the Calcium Looping system.

A sensitivity analysis reveals that changes of ±50% with respect to the reference cases in intrinsic model parameters such as the interchange rate coefficients (K_{bc} and K_{ce}) and the volume of solids in the cloud region divided by the volume of bubbles (γ_c) would hardly affect the final recarbonation conversion. It was also found that the bubble diameter has only a slight effect on the recarbonator efficiency within a range of moderate values, whereas the kinetic constant ($k_{s,R}$) stands out as the most influential parameter of the model, although the effect of this parameter is also restricted given the limited variation observed in recarbonation kinetic experiments. In fact, it is calculated that the recarbonator efficiency diminishes by 19% and increases by 8% when compared to that of the reference case for $k_{s,R}$ values of 0.002 and 0.006 s^{-1} respectively, which correspond to variations of 50 and 150% with respect to the reference $k_{s,R}$.

The model presented in this study is useful for the prediction and interpretation of the performance of a recarbonator, and it can be used as a tool for the design of recarbonator reactors in future Calcium Looping systems for CO_2 capture.

AUTHOR INFORMATION

Corresponding Author

*Corresponding author e-mail address: marlen@incar.csic.es; Tel.:+34 985119090; Fax.: +34 985 297662

ACKNOWLEDGMENT

The financial support provided by the European Community's Research Fund for Coal and Steel under the ReCaL project (RFCR-CT-2012-00008) is acknowledged. M.E. Diego acknowledges the award of a fellowship Grant under the CSIC JAE Programme, co-funded by the European Social Fund.

NOMENCLATURE

A_R = Cross-sectional area of the recarbonator (m^2)

$a_{1,i}$ = Parameter of the recarbonator element i (s^{-1})

$a_{2,i}$ = Parameter of the recarbonator element i

$a_{3,i}$ = Parameter of the recarbonator element i (mol/m^3)

$a_{4,i}$ = Parameter of the recarbonator element i

$a_{5,i}$ = Parameter of the recarbonator element i (mol/m^3)

$C_{b,i}$ = CO_2 molar concentration in the bubble phase of the recarbonator element i (mol/m^3)

$C_{b\ in,i}$ = CO_2 molar concentration in the bubble phase at the inlet of the recarbonator element i (mol/m^3)

$C_{b\ out,i}$ = CO_2 molar concentration in the bubble phase at the outlet of the recarbonator element i (mol/m^3)

$C_{c,i}$ = CO_2 molar concentration in the cloud phase of the recarbonator element i (mol/m^3)

$C_{e,i}$ = CO_2 molar concentration in the emulsion phase of the recarbonator element i (mol/m^3)

C_{eq} = CO_2 molar concentration at equilibrium conditions (mol/m^3)

D = Molecular diffusion coefficient of the gas (m^2/s)

d_b = Bubble diameter (m)

d_p = Mean particle diameter (m)

F_{Ca} = Molar flow of Ca moles between reactors (mol/s)

$F_{CO2,0}$ = Total molar flow of CO_2 fed to the recarbonator reactor (mol/s)

$F_{CO2,carb}$ = Molar flow of CO_2 consumed for the carbonation reaction up to $X_{ave,R}$ inside the recarbonator (mol/s)

$F_{CO2\ in,i}$ = Molar flow of CO_2 that enters the recarbonator element i (mol/s)

$F_{CO2\ out,i}$ = Molar flow of CO_2 that leaves the recarbonator element i (mol/s)

$f_{a,R}$ = Active fraction of particles inside the recarbonator

$f_{Ca\ R,w}$ = Mass fraction of calcium involved in the recarbonation reaction

H_R = Height of the recarbonator reactor (m)

K_{bc} = Gas interchange coefficient between the bubble and the cloud regions (s^{-1})

K_{ce} = Gas interchange coefficient between the cloud and the emulsion regions (s^{-1})

$k_{s,R}$ = Apparent kinetic constant for the recarbonation reaction (s^{-1})

M_s = Molecular weight of the Ca solids (kg/mol)

$n_{Ca,R}$ = Number of calcium moles inside the recarbonator (mol)

T = Temperature (ºC)

t* = Characteristic time of the carbonation reaction after which the reaction rate is zero (s)

t^*_R = Characteristic time of the recarbonation reaction after which the reaction rate is zero (s)

$u_{b,i}$ = Bubble velocity in the recarbonator element i (m/s)

$u_{in,i}$ = Gas velocity at the inlet of the recarbonator element i (m/s)

$u_{out,i}$ = Gas velocity at the outlet of the recarbonator element i (m/s)

u_0 = Total inlet gas velocity to the recarbonator (m/s)

X = CaO carbonate molar conversion

X_{ave} = Average CaO carbonate molar conversion achieved at the end of the fast carbonation period

$X_{ave,R}$ = Average CaO carbonate molar conversion achieved at the end of the fast carbonation period in the presence of a recarbonator reactor

$X_{ave,R}^{+}$ = Average CaO carbonate molar conversion achieved at the end of the fast recarbonation period

X_{carb} = CaO carbonate molar conversion at the exit of the carbonator

X_{CO2} = CO_2 gas conversion

$X_{CO2,i}$ = CO_2 gas conversion inside the recarbonator element i

$X_{CO2,GB}$ = CO_2 gas conversion calculated by means of the gas balance

X_r = Residual conversion of the particles

Z = Number of elements into which the recarbonator reactor is divided for the calculations

z_i = Height at the recarbonator element i (m)

Greek symbols

$\alpha_{c,i}$ = Fraction of solids present in the cloud region of the recarbonator element i

$\alpha_{e,i}$ = Fraction of solids present in the emulsion region of the recarbonator element i

ΔX_R = Increase in the CaO carbonate molar conversion due to recarbonation

$\Delta X_{R,max}$ = Maximum increase in the CaO carbonate molar conversion of the particles due to recarbonation if allowed to progress to the end of the fast recarbonation period

δ_i = Bubble density in the recarbonator element i

ϵ_i = Bed porosity of the recarbonator element i

γ_c = Volume of solids dispersed in the cloud region per volume of bubbles

$\gamma_{e,i}$ = Volume of solids dispersed in the emulsion region per volume of bubbles inside the recarbonator element i

$\rho_{m,g}$ = Molar density of the gas (mol/m^3)

ρ_s = Solids density (kg/m^3)

τ_R = Mean residence time inside the recarbonator (s)

ν = Volume fraction of CO_2 in the gas phase

ν_c = Volume fraction of CO_2 in the cloud region

ν_e = Volume fraction of CO_2 in the emulsion region

ν_{eq} = Volume fraction of CO_2 at equilibrium conditions

$\nu_{in,i}$ = Volume fraction of CO_2 at the inlet of the recarbonator element i

ν_0 = Volume fraction of CO_2 at the inlet of the recarbonator

REFERENCES

(1) Metz, B.; Davidson, O.; Coninck, H.; Loos, M.; Meyer, L. *Special report on carbon dioxide capture and storage*; Intergovernmental Panel on Climate Change. Cambrige University Press: New York, 2005.
(2) Anthony, E. J. Solid Looping Cycles: A New Technology for Coal Conversion. *Ind. Eng. Chem. Res.* **2008,** 47, 1747.
(3) Blamey, J.; Anthony, E. J.; Wang, J.; Fennell, P. S. The calcium looping cycle for large-scale CO_2 capture. *Prog. Energy Combust. Sci.* **2010,** 36, 260.
(4) Shimizu, T.; Hirama, T.; Hosoda, H.; Kitano, K.; Inagaki, M.; Tejima, K. A Twin Fluid-Bed Reactor for Removal of CO_2 from Combustion Processes. *Chem. Eng. Res. Des.* **1999,** 77, 62.
(5) Abanades, J. C.; Alvarez, D. Conversion Limits in the Reaction of CO_2 with Lime. *Energy Fuels* **2003,** 17, 308.
(6) Grasa, G. S.; Abanades, J. C. CO_2 Capture Capacity of CaO in Long Series of Carbonation/Calcination Cycles. *Ind. Eng. Chem. Res.* **2006,** 45, 8846.
(7) Abanades, J. C.; Anthony, E. J.; Wang, J.; Oakey, J. E. Fluidized Bed Combustion Systems Integrating CO_2 Capture with CaO. *Environ. Sci. Technol.* **2005,** 39, 2861.
(8) Romeo, L. M.; Abanades, J. C.; Escosa, J. M.; Paño, J.; Giménez, A.; Sánchez-Biezma, A.; Ballesteros, J. C. Oxyfuel carbonation/calcination cycle for low cost CO_2 capture in existing power plants. *Energy Convers. Manage.* **2008,** 49, 2809.
(9) Romano, M. Coal-fired power plant with calcium oxide carbonation for postcombustion CO_2 capture. *Energy Proc.* **2009,** 1, 1099.
(10) Hawthorne, C.; Trossmann, M.; Galindo Cifre, P.; Schuster, A.; Scheffknecht, G. Simulation of the carbonate looping power cycle. *Energy Proc.* **2009,** 1, 1387.
(11) Yongping, Y.; Rongrong, Z.; Liqiang, D.; Kavosh, M.; Patchigolla, K.; Oakey, J. Integration and evaluation of a power plant with a CaO-based CO_2 capture system. *Int. J. Greenhouse Gas Control* **2010,** 4, 603.
(12) Lasheras, A.; Ströhle, J.; Galloy, A.; Epple, B. Carbonate looping process simulation using a 1D fluidized bed model for the carbonator. *Int. J. Greenhouse Gas Control* **2011,** 5, 686.
(13) Martínez, I.; Murillo, R.; Grasa, G.; Abanades, J. C. Integration of a Ca looping system for CO_2 capture in existing power plants. *AlChE J.* **2011,** 57, 2599.
(14) Lisbona, P.; Martínez, A.; Lara, Y.; Romeo, L. M. Integration of Carbonate CO_2 Capture Cycle and Coal-Fired Power Plants. A Comparative Study for Different Sorbents. *Energy Fuels* **2010,** 24, 728.
(15) Zhao, M.; Minett, A. I.; Harris, A. T. A review of techno-economic models for the retrofitting of conventional pulverised-coal power plants for post-combustion capture (PCC) of CO_2. *Energy & Environmental Science* **2013,** 6, 25.
(16) Abanades, J. C.; Alonso, M.; Rodríguez, N.; González, B.; Grasa, G.; Murillo, R. Capturing CO_2 from combustion flue gases with a carbonation calcination loop. Experimental results and process development. *Energy Proc.* **2009,** 1, 1147.
(17) Lu, D. Y.; Hughes, R. W.; Anthony, E. J. Ca-based sorbent looping combustion for CO_2 capture in pilot-scale dual fluidized beds. *Fuel Process. Technol.* **2008,** 89, 1386.
(18) Charitos, A.; Hawthorne, C.; Bidwe, A. R.; Sivalingam, S.; Schuster, A.; Spliethoff, H.; Scheffknecht, G. Parametric investigation of the calcium looping process for CO_2 capture in a 10 kW_{th} dual fluidized bed. *Int. J. Greenhouse Gas Control* **2010,** 4, 776.

(19) Rodríguez, N.; Alonso, M.; Abanades, J. C. Experimental investigation of a circulating fluidized-bed reactor to capture CO_2 with CaO. *AlChE J.* **2011,** 57, 1356.
(20) Charitos, A.; Rodríguez, N.; Hawthorne, C.; Alonso, M.; Zieba, M.; Arias, B.; Kopanakis, G.; Scheffknecht, G.; Abanades, J. C. Experimental Validation of the Calcium Looping CO_2 Capture Process with Two Circulating Fluidized Bed Carbonator Reactors. *Ind. Eng. Chem. Res.* **2011,** 50, 9685.
(21) Arias, B.; Diego, M. E.; Abanades, J. C.; Lorenzo, M.; Diaz, L.; Martínez, D.; Alvarez, J.; Sánchez-Biezma, A. Demonstration of steady state CO_2 capture in a 1.7MW_{th} calcium looping pilot. *Int. J. Greenhouse Gas Control* **2013,** 18, 237.
(22) Dieter, H.; Hawthorne, H.; Bidwe, A. R.; Zieba, M.; Scheffknecht, G. The 200 kW_{th} Dual Fluidized Bed Calcium Looping Pilot Plant for Efficient CO_2 Capture: Plant Operating Experiences and Results, *21st International Conference on Fluidized Bed Combustion,* Naples (Italy), 3-6 June, **2012**, 397.
(23) Kremer, J.; Galloy, A.; Ströhle, J.; Epple, B. Continuous CO_2 Capture in a 1-MW_{th} Carbonate Looping Pilot Plant. *Chem. Eng. Technol.* **2013,** 36, 1518.
(24) Chang, M. H.; Huang, C. M.; Liu, W. H.; Chen, W. C.; Cheng, J. Y.; Chen, W.; Wen, T. W.; Ouyang, S.; Shen, C. H.; Hsu, H. W. Design and Experimental Investigation of Calcium Looping Process for 3-kW_{th} and 1.9-MW_{th} Facilities. *Chem. Eng. Technol.* **2013,** 36, 1525.
(25) Rodriguez, N.; Alonso, M.; Grasa, G.; Abanades, J. C. Heat requirements in a calciner of $CaCO_3$ integrated in a CO_2 capture system using CaO. *Chem. Eng. J.* **2008,** 138, 148.
(26) Diego, M. E.; Arias, B.; Alonso, M.; Abanades, J. C. The impact of calcium sulfate and inert solids accumulation in post-combustion calcium looping systems. *Fuel* **2013,** 109, 184.
(27) Kierzkowska, A. M.; Pacciani, R.; Müller, C. R. CaO-Based CO_2 Sorbents: From Fundamentals to the Development of New, Highly Effective Materials. *ChemSusChem* **2013,** 6, 1130.
(28) Hughes, R. W.; Lu, D.; Anthony, E. J.; Wu, Y. Improved Long-Term Conversion of Limestone-Derived Sorbents for In Situ Capture of CO_2 in a Fluidized Bed Combustor. *Ind. Eng. Chem. Res.* **2004,** 43, 5529.
(29) Manovic, V.; Anthony, E. J. Steam Reactivation of Spent CaO-Based Sorbent for Multiple CO_2 Capture Cycles. *Environ. Sci. Technol.* **2007,** 41, 1420.
(30) Zeman, F. Effect of steam hydration on performance of lime sorbent for CO_2 capture. *Int. J. Greenhouse Gas Control* **2008,** 2, 203.
(31) Phalak, N.; Wang, W.; Fan, L. S. $Ca(OH)_2$-Based Calcium Looping Process Development at The Ohio State University. *Chem. Eng. Technol.* **2013,** 36, 1451.
(32) Arias, B.; Grasa, G. S.; Abanades, J. C. Effect of sorbent hydration on the average activity of CaO in a Ca-looping system. *Chem. Eng. J.* **2010,** 163, 324.
(33) Yu, F.-C.; Phalak, N.; Sun, Z.; Fan, L.-S. Activation Strategies for Calcium-Based Sorbents for CO_2 Capture: A Perspective. *Ind. Eng. Chem. Res.* **2011,** 51, 2133.
(34) Lysikov, A. I.; Salanov, A. N.; Okunev, A. G. Change of CO_2 Carrying Capacity of CaO in Isothermal Recarbonation−Decomposition Cycles. *Ind. Eng. Chem. Res.* **2007,** 46, 4633.
(35) Manovic, V.; Anthony, E. J. Thermal Activation of CaO-Based Sorbent and Self-Reactivation during CO_2 Capture Looping Cycles. *Environ. Sci. Technol.* **2008,** 42, 4170.
(36) Manovic, V.; Anthony, E. J.; Grasa, G.; Abanades, J. C. CO_2 Looping Cycle Performance of a High-Purity Limestone after Thermal Activation/Doping. *Energy Fuels* **2008,** 22, 3258.
(37) Manovic, V.; Anthony, E. J.; Loncarevic, D. CO_2 looping cycles with CaO-based sorbent pretreated in at high temperature. *Chem. Eng. Sci.* **2009,** 64, 3236.

(38) Chen, Z.; Song, H. S.; Portillo, M.; Lim, C. J.; Grace, J. R.; Anthony, E. J. Long-Term Calcination/Carbonation Cycling and Thermal Pretreatment for CO_2 Capture by Limestone and Dolomite. *Energy Fuels* **2009,** 23, 1437.
(39) Ozcan, D. C.; Shanks, B. H.; Wheelock, T. D. Improving the Stability of a CaO-Based Sorbent for CO_2 by Thermal Pretreatment. *Ind. Eng. Chem. Res.* **2011,** 50, 6933.
(40) Arias, B.; Abanades, J. C.; Anthony, E. J. Model for Self-Reactivation of Highly Sintered CaO Particles during CO_2 Capture Looping Cycles. *Energy Fuels* **2011,** 25, 1926.
(41) Arias, B.; Grasa, G. S.; Alonso, M.; Abanades, J. C. Post-combustion calcium looping process with a highly stable sorbent activity by recarbonation. *Energy & Environmental Science* **2012**.
(42) Abanades, J. C.; Arias, B.; Grasa, G. Device and method for the capture of CO_2 by CaO carbonation and for mantaining sorbent activity. PCT/ES2012/070426, 2012.
(43) Barker, R. The reversibility of the reaction $CaCO_3 \rightleftarrows CaO+CO_2$. *Journal of applied chemistry & biotechnology* **1973,** 23, 733.
(44) Sun, P.; Lim, C. J.; Grace, J. R. Cyclic CO_2 capture by limestone-derived sorbent during prolonged calcination/carbonation cycling. *AlChE J.* **2008,** 54, 1668.
(45) Anthony, E. J.; Bulewicz, E. M.; Jia, L. Reactivation of limestone sorbents in FBC for SO_2 capture. *Prog. Energy Combust. Sci.* **2007,** 33, 171.
(46) Anthony, E. J.; Lu, D.; Salvador, C. Reactivation of lime-based sorbents by CO_2 shocking. US 7,879,139 B2, 2011.
(47) Grasa, G.; Martínez, I.; Diego, M. E.; Abanades, J. C. Determination of carbonation kinetics of CaO under recarbonation conditions. *Energy Fuels* **In press**.
(48) Kunii, D.; Levenspiel, O. Fluidized reactor models. 1. For bubbling beds of fine, intermediate, and large particles. 2. For the lean phase: freeboard and fast fluidization. *Ind. Eng. Chem. Res.* **1990,** 29, 1226.
(49) Diego, M. E.; Arias, B.; Abanades, J. C. Modeling the solids circulation rates and solids inventories of an interconnected circulating fluidized bed reactor system for CO_2 capture by calcium looping. *Chem. Eng. J.* **2012,** 198–199, 228.
(50) Liljedahl, G. N.; Turek, D. G.; ya Nsakala, N.; Mohn, N. C.; Fout, T. E., Alstom's Oxygen-Fired CFB Technology Development Status for CO_2 Mitigation. In *31st International Technical Conference on Coal Utilization & Fuel Systems*, Clearwater, Florida, USA, 2006.
(51) Manovic, V.; Anthony, E. J. Carbonation of CaO-Based Sorbents Enhanced by Steam Addition. *Ind. Eng. Chem. Res.* **2010,** 49, 9105.
(52) Donat, F.; Florin, N. H.; Anthony, E. J.; Fennell, P. S. Influence of High-Temperature Steam on the Reactivity of CaO Sorbent for CO_2 Capture. *Environ. Sci. Technol.* **2011,** 46, 1262.
(53) Davidson, J. F.; Harrison, D. *Fluidized Particles*; Cambridge University Press: New York, 1963.
(54) Bhatia, S. K.; Perlmutter, D. D. Effect of the product layer on the kinetics of the CO_2-lime reaction. *AlChE J.* **1983,** 29, 79.
(55) Silaban, A. High temperature capture of carbon dioxide: characteristics of the reversible reaction between CaO(s) and CO2(g). *Chem. Eng. Commun.* **1995,** 137, 177.
(56) Mess, D.; Sarofim, A. F.; Longwell, J. P. Product Layer Diffusion during the Reaction of Calcium Oxide with Carbon Dioxide. *Energy Fuels* **1999,** 13, 999.
(57) Abanades, J. C. The maximum capture efficiency of CO_2 using a carbonation/calcination cycle of $CaO/CaCO_3$. *Chem. Eng. J.* **2002,** 90, 303.

(58) Alonso, M.; Rodríguez, N.; Grasa, G.; Abanades, J. C. Modelling of a fluidized bed carbonator reactor to capture CO_2 from a combustion flue gas. *Chem. Eng. Sci.* **2009,** 64, 883.
(59) Levenspiel, O. *Chemical Reaction Engineering*; Wiley: 1999.
(60) Romano, M. C. Modeling the carbonator of a Ca-looping process for CO_2 capture from power plant flue gas. *Chem. Eng. Sci.* **2012,** 69, 257.
(61) Li, Z.-s.; Cai, N.-s.; Croiset, E. Process analysis of CO_2 capture from flue gas using carbonation/calcination cycles. *AlChE J.* **2008,** 54, 1912.
(62) Hawthorne, C.; Charitos, A.; Perez-Pulido, C. A.; Bing, Z.; Scheffknecht, G. Design of a dual fluidised bed system for the post-combustion removal of CO_2 using CaO. Part I: CFB carbonator reactor model. *9th International Conference on Circulating Fluidized Beds (Hamburg, Germany)* **2008**.
(63) Romeo, L. M.; Lara, Y.; Lisbona, P.; Escosa, J. M. Optimizing make-up flow in a CO_2 capture system using CaO. *Chem. Eng. J.* **2009,** 147, 252.
(64) Abanades, J. C.; Arias, B.; Diego, M. E.; Martínez, I. System for CO_2 capture from a combustion flue gas using a $CaO/CaCO_3$ chemical loop. EP13382206.